Intensely swirling turbulent pipe flow downstream of an orifice: the influence of an outlet contraction

Marcel Escudier[1], Keith Nickson[2], Robert Poole[3]
1: Department of Engineering, University of Liverpool, Liverpool, UK, escudier@liv.ac.uk
2: Department of Engineering, University of Liverpool, Liverpool, UK, k.nickson@liv.ac.uk
3: Department of Engineering, University of Liverpool, Liverpool, UK, robpoole@liv.ac.uk

Abstract Detailed laser Doppler anemometry (LDA) measurements are reported on the influence of an outlet contraction on swirling turbulent pipe flow downstream of an orifice. Two levels of swirl are investigated, both sufficiently high for vortex breakdown to occur just downstream of the orifice. At the lower level of swirl, the flow downstream of breakdown is supercritical while for the higher level it is subcritical. The outcome of this research is a large database of detailed velocity and turbulence measurements for two different outlet geometries, fully open and a concentric central contraction, which include the mean axial and tangential velocity distributions and the corresponding streamline patterns. For the low-swirl case ($S \approx 0.3$) the flow is largely unaffected by a central contraction placed several diameters downstream of the inlet orifice confirming that this flow is supercritical downstream. A closed recirculation bubble (vortex breakdown) occurs centred on the axis just downstream of the inlet. Downstream of this bubble the swirl decays as does the central wake-like deficit in the axial velocity. The high-swirl case ($S \approx 0.6$) is much more complex and the flows with and without the contraction are completely different. In the absence of the contraction there is backflow throughout the vortex core and no closed recirculation region. With the contraction in place, a closed recirculation region is again found centred on the axis but considerably distorted when compared with the "simple" elongated smooth shape of the low-swirl vortex breakdown. Downstream of this recirculation region, as the swirl decays, a growing overshoot is found on axis. The strong influence of the outlet contraction confirms that the high-swirl cases are subcritical in the downstream region. In all cases that there is an outer annular region of recirculation just downstream of the orifice plate, much as would be the case in the absence of swirl. For each of the flows investigated, the vortex core showed no sign of distortion with axial position or precession.

Introduction

Detailed LDA measurements are reported on the influence of an outlet contraction on swirling turbulent pipe flow downstream of an orifice. Two levels of swirl are investigated, both sufficiently high for vortex breakdown to occur just downstream of the orifice. At the lower level of swirl, the flow downstream of breakdown is supercritical while for the higher level it is subcritical. Measurements include the mean axial and tangential velocity distributions and the corresponding streamline patterns. It has been known for some time (e.g Escudier and Keller (1985), Hogg and Leschziner (1989)) that swirling flows which remain subcritical downstream of breakdown are sensitive to outlet conditions many pipe diameters downstream. There are numerous examples of numerical "predictions" of such flows in which the outlet velocity profile is prescribed rather than calculated. In other cases the problem is avoided by artificially extending the computational domain (e.g Kim et al (1999)) or simply ignored (e.g Yaras and Grosvenor (2003)). The paucity of experimental data with which to compare calculations or develop methods to deal with the subcritical outlet boundary-condition problem has motivated the present study.

Experimental details

The flow geometry is shown schematically in **Figure 1**. Swirl is generated using a tangential-slit arrangement which is a refinement of the single-slit geometry used by Escudier, Bornstein and Zehnder (1980). In the present set up, water flows through 12 tangential inlet slits each 1 mm wide

which discharge into a 12-sided pipe for which the diameter of the inscribed circle is 55 mm (see the insert in **Figure 1**). Flow from the swirl generator passes into a co-axial circular pipe of diameter D = 55 mm in which the LDA measurements reported here were made. A circular inlet orifice of diameter D_E = 25 mm was installed in the pipe 175 mm from the outlet of the swirl generator. For the low-swirl case, vortex breakdown occurs 10 mm downstream of this orifice. The location of the breakdown was set by adjusting the swirl level by varying the open length L of the slits. A crude measure of the swirl intensity is given by the geometric parameter (see Escudier, Bornstein and Zehnder (1980)) $\Omega = \pi^2D^2/4ntL$, where n is the number of slits (i.e 12) and t the slot width (1 mm). The low level of swirl results from L = 95 mm and the high level from L = 35 mm. The usual definition of the swirl parameter S is

$$S = \frac{2A_E}{M_E D_E}$$

where A_E is the axial momentum flowrate through the inlet

$$A_E = 2\pi\int_0^{R_E} \rho uvr^2 dr$$

and M_E is the axial flowrate of angular momentum

$$M_E = 2\pi\int_0^{R_E} \rho u^2 r dr$$

For the low-swirl and high-swirl situations, the values of S are about 0.3 and 0.6, respectively. The pipe-flow Reynolds number U_BD/ν was about 1550 in all cases, where U_B is the bulk axial velocity in the pipe. Based upon the orifice flow, the Reynolds number U_ED_E/ν was about 3400, where U_E is the average axial velocity through the inlet orifice. The pipe outlet is 470 mm (8.5 pipe diameters) from the plane of the orifice plate and the flow discharges into a large collection tank within which the water level is below that of the outlet so that the outlet condition is that of a free surface. For each of the two swirl-parameter values, measurements are reported here for two outlet conditions: fully open and with a 25 mm contraction installed 330mm (6 pipe diameters) from the inlet orifice. The location of the outlet contraction was chosen to match the experimental arrangement of Escudier and Keller (1985).

The measurements were carried out in forward scatter using a Dantec Fibreflow LDA system comprising a 60X10 probe and 57X08 receiving optics. The beam separation at the front lens was 51.5 mm and the lens focal length 160 mm which produced a measuring volume 0.28 mm long and 0.045 mm in diameter. The signals were processed using a Dantec Particle Dynamics Analyser, model 58N10. Flow rates were measured using an Endress & Hauser Promass 60 mass flowmeter.

Experimental results

a) Low swirl

Streamlines were constructed from values of the stream function $\psi = 2\pi\int_0^R urdr$ calculated from the measured radial distributions of the mean axial velocity component u. For each of the two low-swirl situations, the streamline patterns are shown in **Figure 2** with the axial-velocity profiles superimposed the ♦ symbols denote the locations of zero axial velocity. The streamline maps reveal two closed areas of recirculation. There is an elongated recirculation bubble centred on the pipe axis and starting slightly downstream of the orifice, indicative of vortex breakdown. The outer toroidal region of recirculation immediately downstream of the orifice is a consequence of the sudden area expansion. The reattachment length is about 40 mm (x/D = 0.73) or slightly less than three step heights. The flow is practically unaffected by the outlet geometry which is fully open for **Figure 2(a)** and a 25 mm central contraction (i.e 79% area reduction) 330 mm from the inlet orifice for **Figure 2(b)**. We interpret the insensitivity of the flow to the outlet condition as indicating that

the flow is supercritical, i.e that the propagation speed of longitudinal inertia waves is lower than the average axial flowspeed. A more precise determination of whether an experimental flow is supercritical or subcritical, e.g using Benjamin's (1962) critical equation, is practically impossible.

The swirl profiles v(r) for the fully-open outlet (the profiles for the contraction outlet are practically identical) are shown superimposed in **Figure 3**. The profiles for all axial locations are shown on the right-hand side of the figure, selected profiles on the left. Several key features of the flow are apparent from this form of presentation**:** the swirl profiles reveal a quadruple structure comprising an inner core within which the swirl velocity progressively decays, an outer envelope extending to 0.4R, an outer region to about 0.9R where the flow is probably influenced by large-scale Goertler vortices, and a near-wall boundary layer. The peak swirl velocity in the vortex core decays from about $5.5U_B$ at exit from the inlet orifice to about $0.5U_B$ one diameter downstream and beyond. As the swirl decays, the core radius (measured as the radial distance to the swirl-velocity peak) increases progressively from about 0.1R to 0.6R. Further decay of the swirl profile beyond one diameter downstream of the inlet orifice is imperceptible.

The corresponding variation of the axial-velocity component u(r) shown in **Figure 4** is far more complex. Between the inlet orifice and x = 10 mm (x/D = 0.18) the axial velocity is jet like within the vortex core with a peak velocity on the centreline of about $9U_B$ though this decays rapidly to a wake-like form further downstream becoming negative at about x = 12 mm (x/D = 0.22) with a maximum reverse-flow velocity, on the axis at x = 17.5 mm of about $-2U_B$. The recirculation evident in the streamline plots corresponds to the combination of these negative core velocities and the positive axial velocities surrounding the core with peaks reaching $5.5U_B$. The progressive change to forward flow over most of the tube cross section downstream of the recirculation bubble is apparent though the wake-like deficit on the centreline is still evident at the last measuring location but clearly diminishing. The centreline velocity here is still 25% lower than the peak velocity (at about r/R = 0.8)

b) High swirl

In contrast to the supercritical flow case, the streamline patterns for the high-swirl situation are entirely different for the two exit conditions which we take to indicate that the downstream flows are subcritical. For the fully-open case, **Figure 5(a),** there is reverse flow along the vortex core all the way to the inlet orifice and, in fact, even penetrating into the region upstream of the inlet orifice. The outer toroidal region of recirculation is considerably shorter than for the low-swirl case (reattachment length about 25 mm (x/D = 0.45) compared with 40 mm(x/D = 0.73)). The shorter reattachment length is associated with a bulge in the streamline patterns within one diameter of the inlet orifice. The bulge does not close as in the supercritical case to form a recirculation "bubble" but the streamlines initially converge downstream and then stay more or less cylindrical throughout the measurement zone. The ♦ symbols denote the locations of zero axial velocity. Within the boundary set by the locus of these points there is reverse flow all the way to (and beyond) the orifice (see below).

With the outlet contraction installed, **Figure 5(b),** there is a central region of recirculation in the near vicinity (x < D) of the inlet orifice and a jet-like flow further downstream (beyond one diameter from the inlet orifice). This recirculation zone exhibits some of the characteristics of vortex breakdown, such as recirculation with reverse flow along the axis, but is clearly far more complex in structure than the well defined bubbles shown in **Figure 2**. The outer recirculation zone is again shorter (ca 27 mm (x/D = 0.49) than for the low-swirl case.

The swirl profiles for the fully-open exit (**Figure 6(a)**) and for the outlet contraction (**Figure 6(b)**) show both similarities and differences**.** An important qualitative difference is seen at the first measurement location for the contraction case the core profile is practically linear (solid-body rotation) much as for the low-swirl flows whereas the fully-open case exhibits a central inflection within r/R ≈ 0.1. In both cases, the peak swirl velocity is about $7U_B$ at r/R = 0.3 at the first measuring location (x = 5 mm) and decreases progressively as the core broadens until about x = 20 mm (x/D = 0.36). The swirl profiles are similar in form until about x = 15 mm but further downstream the two cases are qualitatively quite different. For the fully-open case the swirl profiles continue to decay but at a much reduced rate and are broadly self similar throughout the remaining measuring region. For the outlet contraction, however, within the central core region the profiles are almost identical beyond x = 5 mm but steeper than the profile at x = 5 mm and almost identical across the entire cross section downstream of the decay region (i.e beyond x = 20 mm). The more complex profile shapes for both cases in the upstream region (x/D > 0.4) are a consequence of the interdependence with the axial flowfield.

As expected from the streamline patterns, the axial-flow profiles shown in **Figure 7** reveal complex and different behaviour for the two cases, although there are still some similarities. The profiles for the two cases are almost identical until x = 20 mm with reverse flow on the centreline decreasing from about $-3U_B$ to $-U_B$. At x = 25 mm, however, the profiles for the two cases become markedly different. Although it could not be measured, it has to be assumed that there is reverse flow upstream of the inlet orifice, possibly even within the swirl generator which is about three diameters upstream of the orifice. Such behaviour has been observed in gas-turbine combustor swirlers (Syed (2004)). As was seen in **Figure 5(a)**, for the fully-open case there is reverse flow throughout the measuring region whereas for the contraction flow the flow becomes progressively more jet like with downstream distance. The axial profiles show that the change from reverse to forward flow occurs at about x = 40 mm (x/D = 0.73). The complexity of the flow between about x = 27.5 mm (x/D = 0.5) and x = 45 mm explains the difficulty encountered in attempting to construct the streamlines shown in **Figure 5(b).**

In all four cases, the mean flows remained axisymmetric and steady with no evidence of distortion or precession of the vortex core. For other downstream conditions, not discussed here, such as an offset outlet contraction, the core was found to be no longer straight but distorted along its length although still fixed in space (i.e not precessing).

Conclusions

Detailed LDA measurements of the mean axial and swirl components of velocity have been reported for swirling turbulent pipe flows as they develop downstream of a sudden expansion. For the low-swirl case (S ≈ 0.3) the flow is largely unaffected by a central contraction placed six diameters downstream of the inlet orifice confirming that this flow is supercritical downstream. A closed recirculation bubble (vortex breakdown) occurs centred on the axis just downstream of the inlet. Downstream of this bubble the swirl decays as does the central wake-like deficit in the axial velocity. The high-swirl case (S ≈ 0.6) is much more complex and the flows with and without the contraction are completely different. In the absence of the contraction there is backflow throughout the vortex core and no closed recirculation region. With the contraction in place, a closed recirculation region is again found centred on the axis but considerably distorted when compared with the "simple" elongated smooth shape of the low-swirl vortex breakdown. Downstream of this recirculation region, as the swirl decays, a growing overshoot is found on axis. The strong influence of the outlet contraction confirms that the high-swirl cases are subcritical in the downstream region. In all cases that there is an outer annular region of recirculation just

downstream of the orifice plate, much as would be the case in the absence of swirl. For each of the flows investigated, the vortex core showed no sign of distortion with axial position or precession.

References

T B Benjamin "Theory of the vortex breakdown phenomenon" J Fluid Mech Vol 14, No 4, pp 593-629 (1962)

M P Escudier and J J Keller "Recirculation in swirling flows: a manifestation of vortex breakdown" AIAA J Vol 23, No 1, pp 1111-116 (1985)

M P Escudier, J Bornstein and N Zehnder "Observations and LDA measurements of confined turbulent vortex flow" J Fluid Mech Vol 98, No 1, pp 49-63 (1980)

S Hogg and M A Leschziner "Computation of highly swirled confined flow with a Reynolds stress turbulence model" AIAA J Vol 27, No 1, pp 57-63 (1989)

W-W Kim, S Menon and H C Mongia "Large-eddy simulation of a gas turbine combustor flow" Combust Sci and Tech Vol 143, pp 25-62 (1999)

K Syed, Siemens Gas Turbines Ltd Private communication. (2004)

M I Yaras and A D Grosvenor "Evaluation of one- and two0-equation low-*Re* turbulence models. Part I – Axisymmetric separating and swirling flows" Int J Num Meth Fluids Vol 42, pp 1293-1319 (2003)

Figure Captions

Figure 1. Schematic diagram of vortex tube arrangement with details of swirl generator inset

Figure 2. Streamline patterns constructed from axial-velocity distributions with axial-velocity profiles superimposed (a) S = 0.3, fully open outlet (b) S = 0.34, 25 mm ϕ outlet contraction , ♦ denotes zero axial velocity, ■ a stagnation point and ▬ $\psi = 0$

Figure 3. Radial distributions of mean swirl velocity at all x-locations for S = 0.3, fully-open outlet.

Figure 4. Radial distributions of mean axial velocity at all x-locations for S = 0.3, fully-open outlet

Figure 5. Streamline patterns and axial-velocity profiles with axial-velocity profiles superimposed (a) S = 0.6, full-open outlet (b) S = 0.61, 25 mm ϕ outlet contraction, ♦ denotes zero axial velocity, ■ a stagnation point and ▬ $\psi = 0$

Figure 6. Radial distributions of mean swirl velocity at all x-locations for (a) S = 0.6, fully-open outlet (b) S = 0.61, 25 mm ϕ outlet contraction

Figure 7. Radial distributions of mean axial velocity at all x-locations for (a) S = 0.6, fully-open outlet (b) S = 0.61, 25 mm ϕ outlet contraction

21st April 2006

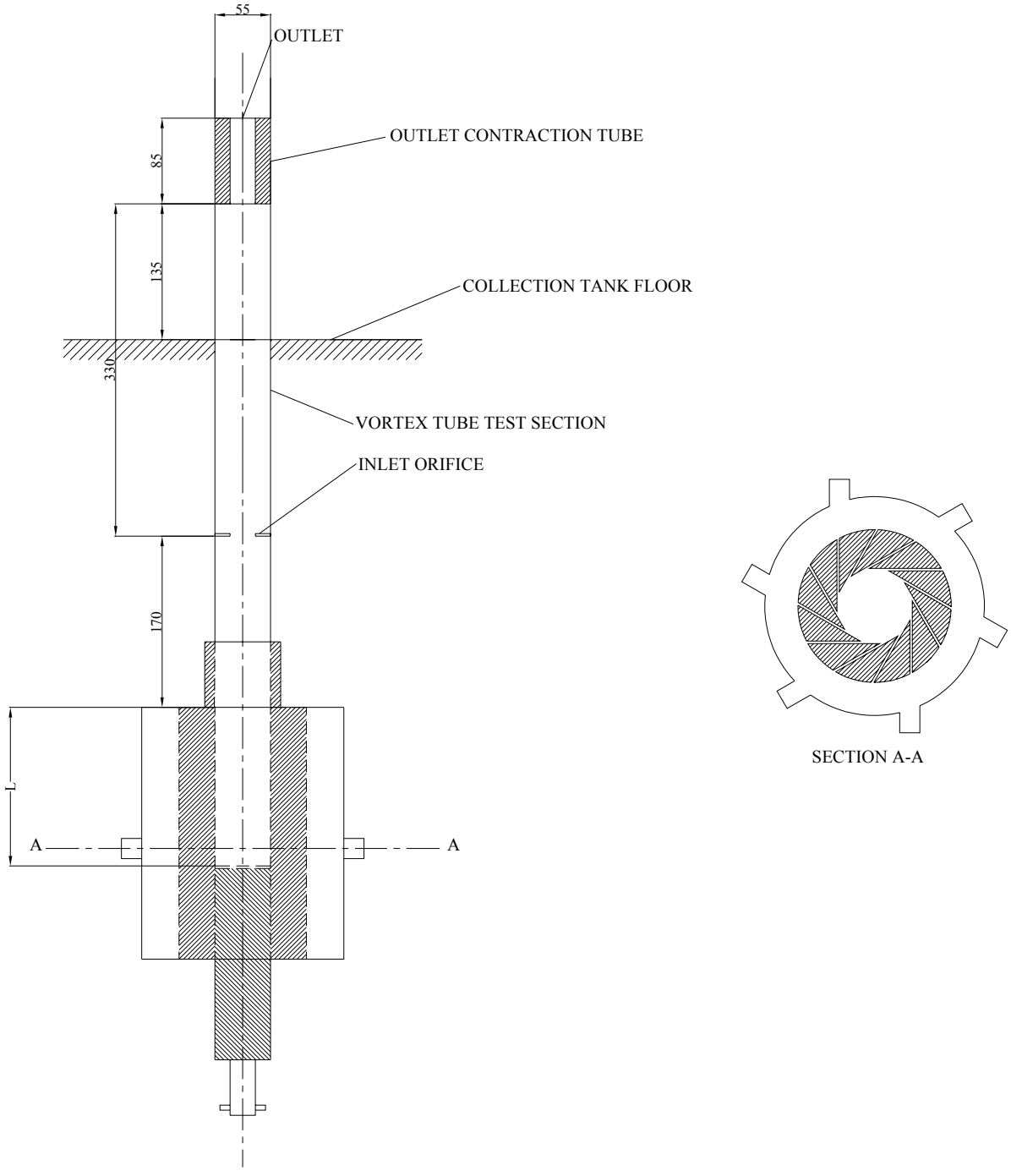

Figure 1. Schematic diagram of vortex tube arrangement with details of swirl generator inset (dimensions in mm).

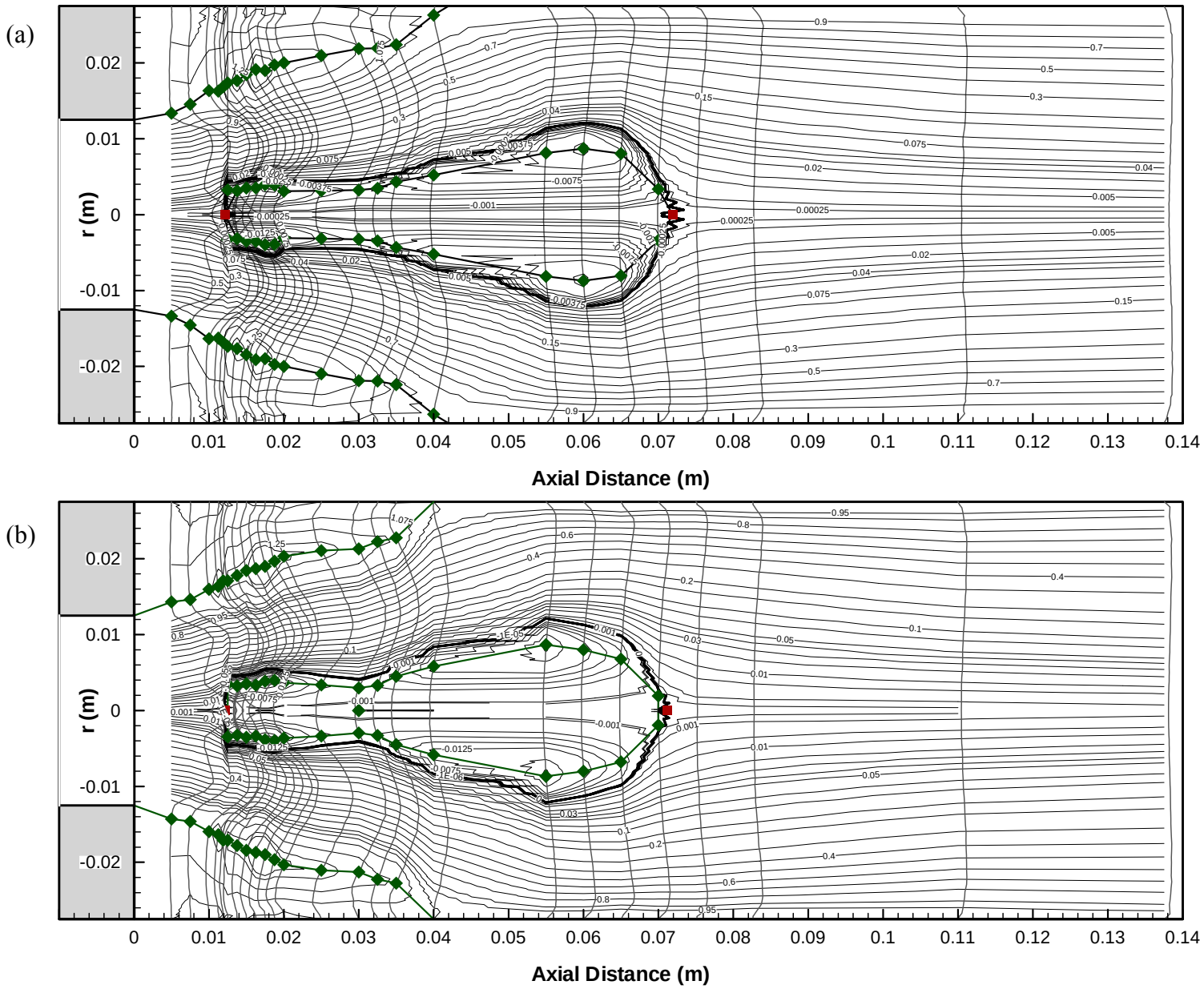

Figure 2. Streamline patterns constructed from axial-velocity distributions with axial-velocity profiles superimposed (a) S = 0.3, fully-open outlet (b) S = 0.34, 25mm ϕ outlet contraction, ◆ denotes zero axial velocity, ■ a stagnation point and ▬ ψ = 0

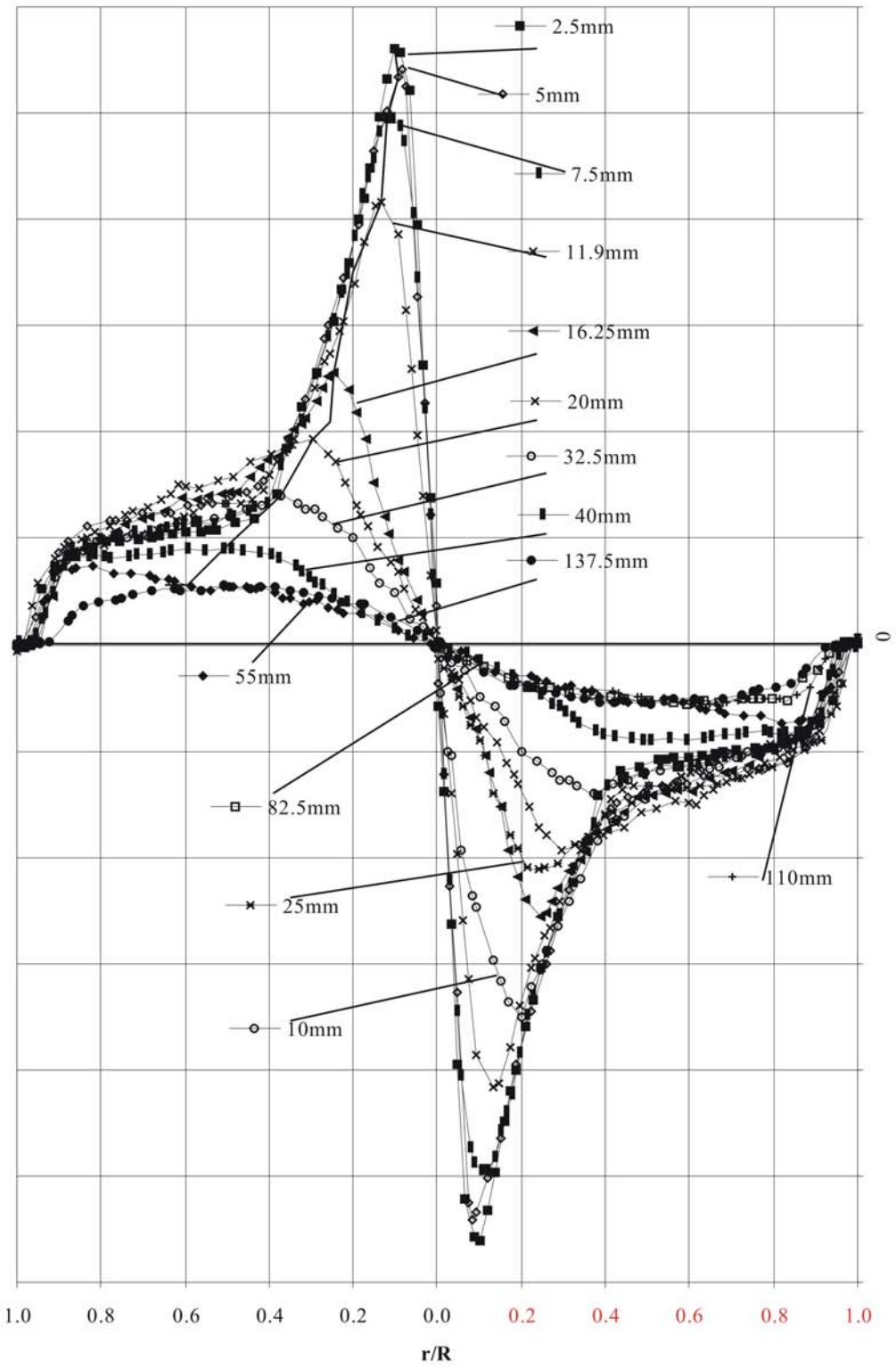

Figure 3. Radial distributions of mean swirl velocity at all x-locations for S = 0.3, fully-open outlet

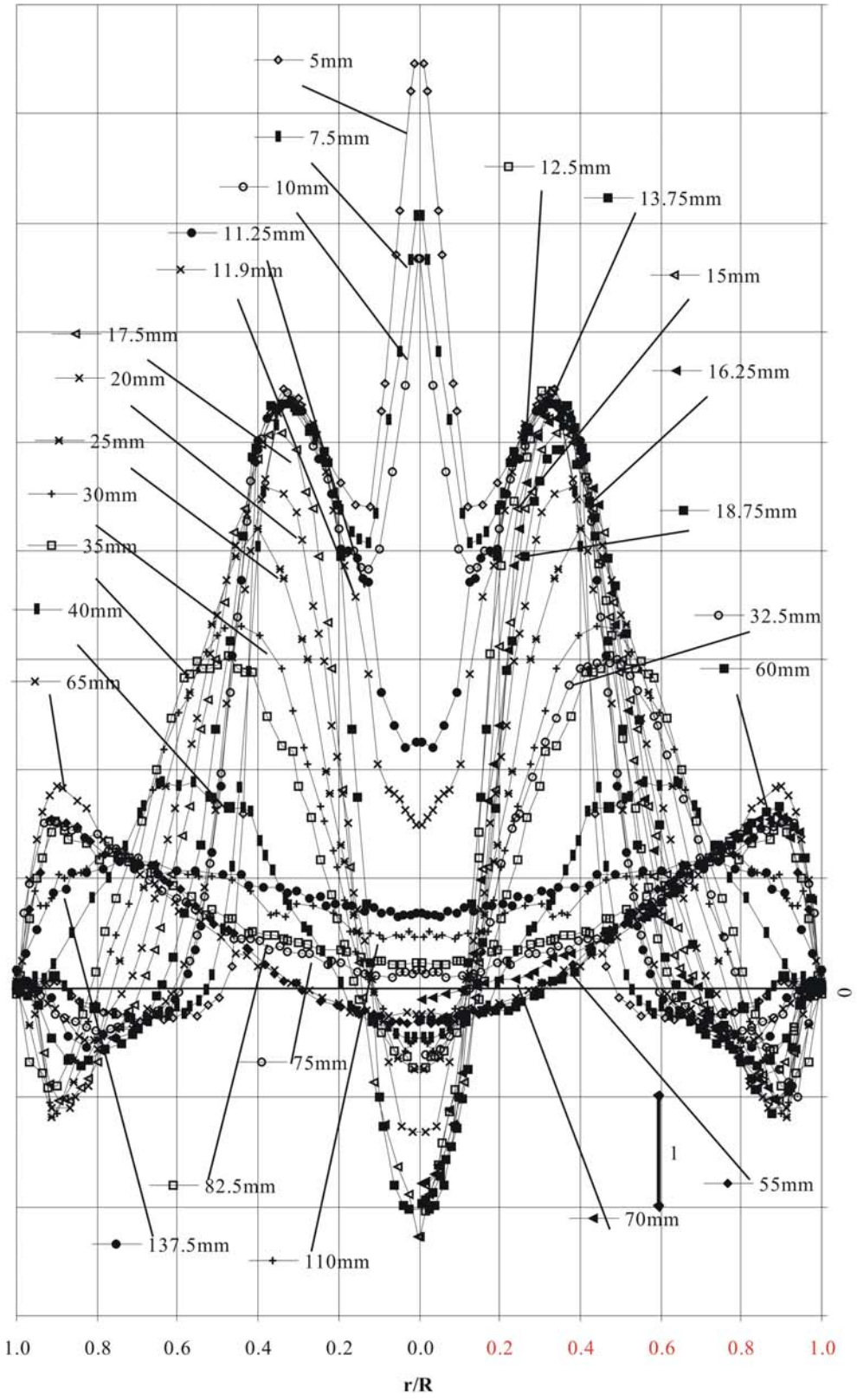

Figure 4. Radial distributions of mean axial velocity at all x-locations for S = 0.3, fully-open outlet

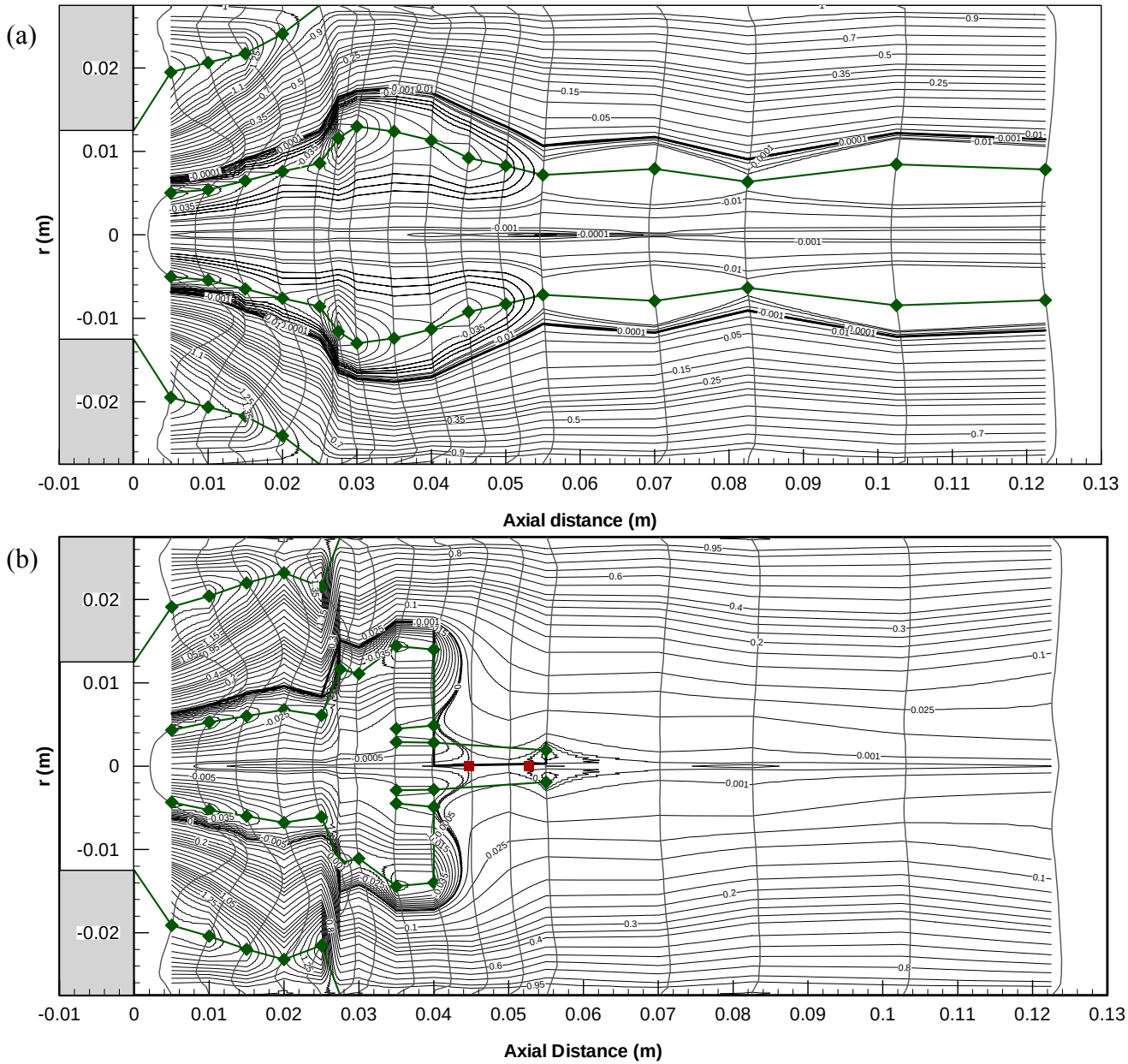

Figure 5. Streamline patterns constructed from axial-velocity distributions with axial-velocity profiles superimposed (a) S = 0.6, fully-open outlet (b) S = 0.61, 25mm ϕ outlet contraction, ◆ denotes zero axial velocity, ■ a stagnation point and ▬ $\psi = 0$

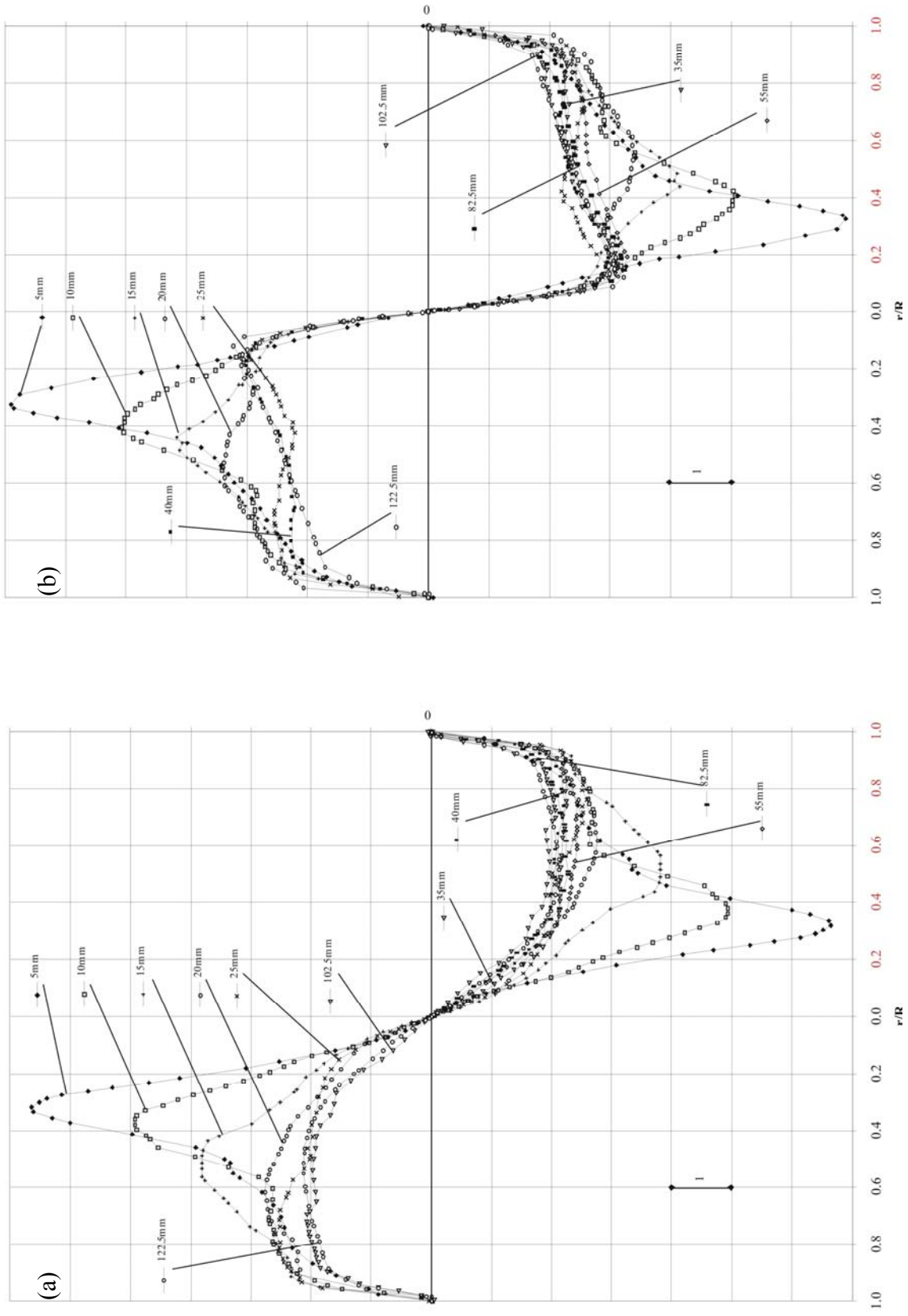

Figure 6. Radial distributions of mean swirl velocity at all x-locations for (a) S = 0.6, fully-open outlet (b) S = 0.61, 25mm ϕ outlet contraction

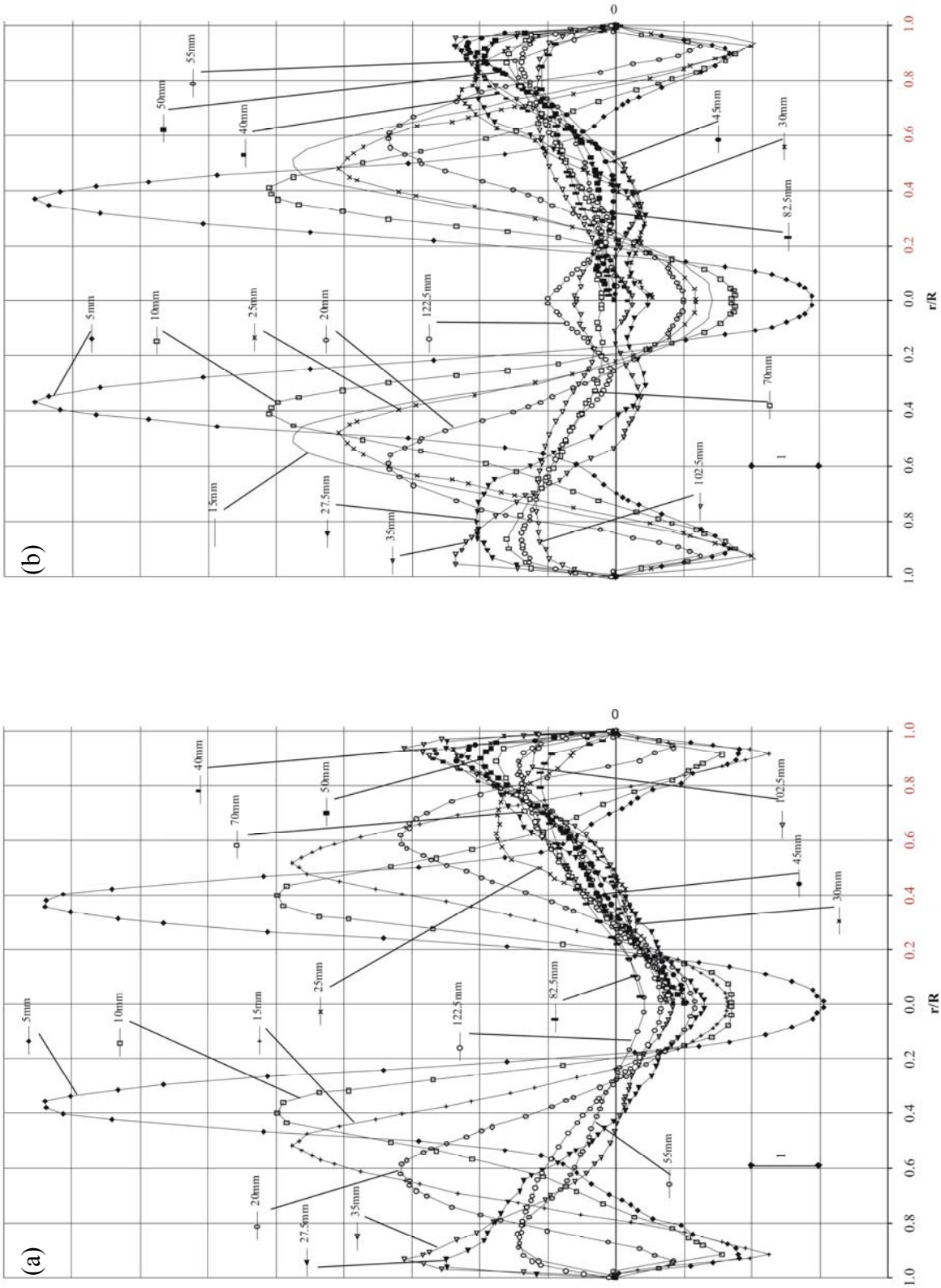

Figure 7. Radial distributions of mean axial velocity at all x-locations for (a) S = 0.6, fully-open outlet (b) S = 0.61, 25mm ϕ outlet contraction